Photosensitivity of barium germano-gallate glasses under femtosecond laser direct writing for Mid-IR applications

Heng Yao, Rayan Zaiter, Maxime Cavillon, Benjamin Sapaly, Florian Calzavara, Pierre Delullier, Thierry Cardinal, Ye Dai, Bertrand Poumellec, Matthieu Lancry

Photosensitivity of Barium Germano-Gallate Glasses under Femtosecond Laser Direct Writing for Mid-IR Applications

Heng Yao[1,2], Rayan Zaiter[3], Maxime Cavillon[2], Benjamin Sapaly[2], Florian Calzavara[3], Pierre Delullier[1,4], Thierry Cardinal[3], Ye Dai[1,†], Bertrand Poumellec[2], and Matthieu Lancry[2,*]

[1] Department of Physics, Shanghai University, Shanghai 200444, China

[2] Institut de Chimie Moléculaire et des Matériaux d'Orsay, SP2M, CNRS, Université Paris-Saclay, 91405 Orsay, France

[3] Université de Bordeaux, CNRS, ICMCB, UPR 9048, F-33608 Pessac, France

[4] ONERA-The French Aerospace Lab., Palaiseau F-91761, France

Corresponding authors: † yedai@shu.edu.cn

* matthieu.lancry@universite-paris-saclay.fr

Abstract

Barium germano-gallate glasses are attractive glass hosts for photonic applications in the mid-infrared region up to 6 µm. In this work, we investigate the photosensitivity of such glasses under femtosecond laser, with an emphasize on the formation of refractive index changes. Six glasses with varying compositions (including addition of K, Na, Y, and La) were studied. We observed several transformation regimes in the pulse energy – repetition rate landscape: Type I (isotropic refractive index change) and a spatial broadening regime with a phase shift $\Delta\varphi > 2\pi$ rad at 550 nm. This translates into refractive index changes $\Delta n > 10^{-2}$ and is comparable to values obtained in most chalcogenide glasses. The effect of glass composition on $\Delta\varphi$ appears correlated to the number of non-bridging oxygen presented in the glass and is brought to evidence by monitoring the Cations/$GaO_{3/2}$ ratio. This provides a way to design a range of germano-gallate glasses suitable to imprinting high refractive index contrast.

Keywords: Barium germano-gallate glass; K/Na/Y/La doping; Femtosecond laser; Refractive index change

1. Introduction

Femtosecond (fs) laser direct writing (FLDW) is a versatile tool that enables permanent modifications of physical properties inside transparent materials, including glass, polymer and crystal [1]. FLDW is achieved by focusing an fs-laser beam on or below the surface of transparent materials. The tightly focused light can reach intensities of several TW/cm^2, yielding to nonlinear light absorption and permanent transformations of the pristine glass within few μm^3 in and around the laser focal volume. Consequently, this technique has attracted attention in fields such as, but not limited to, optomechanics, integrated photonics, graded index and diffractive optics for laser, spectroscopy and imaging applications [2-10].

The most ubiquitous glass materials employed for FLDW are silica and silicate (i.e., silica-rich glasses) [11], as they are readily available and offer both excellent optical transparency and chemical stability. However, for photonic applications, these glasses are limited to the short-wavelength-IR range (SWIR, < 3 μm). This intrinsic limitation prevents their use in applications requiring longer wavelengths. This operating wavelength window is interesting in the 3D manufacturing of miniaturized, low weight and cost optical systems, for civilian (domotics, smartphone, automobile) but also security and military applications (vehicles steering, survey, weapons guidance, unmasking, countermeasure identification). Hence, to circumvent this restriction imposed by silica / silicate glasses and access the Mid-infrared (Mid-IR) range (up to 5-8 μm), non-silicate glass matrices must be employed, such as chalcogenides [12-14], fluorides [15], or heavy oxides [16]. Among these potential candidates, heavy metal oxide (HMO) glasses can exhibit an extended transmission in the IR range up to 7-8 μm. More specifically barium gallo-germanate (BGG) glasses, appear as materials of choice since they are chemically stable, manufacturable by conventional means (melt-quenching) and mechanically resistant [3]. Moreover, hydroxyl impurities could be eliminated by a purification method based on halogens, which produce gallo-germanate glasses with improved transparency up to ~6 μm [17].

The gallo-germanate glass family has already been investigated for a series of optical applications, including high-energy Mid-IR laser output windows [18], waveguides [3], or as active optical fiber hosts [19, 20]. Although this glass family has shown a consequent potential, it still must be photosensitive to laser fs-light in order to imprint

specific functions. Shortly, in silica glass, which is the most common glass material investigated by the community, there exists three types of fs-laser induced modifications. They are commonly referred in the literature as IR-fs Type I, Type II and Type III, respectively [5, 21, 22]. Type I is generally observed at low pulse energies, and is characterized by a smooth and homogeneous structural modification beyond a given threshold [5]. It is also worth noting that composition fluctuation has little impact on the Type I threshold [23]. The expected material response is a permanent and isotropic refractive index variation: these conditions are desired for applications like optical waveguide or lenses. Type II regime is generally observed for slightly higher deposited energies, and is characterized by the formation of birefringent self-assembled periodic nanostructures [21]. Finally, the Type III regime is reached when the intensity of pulse energy exceeds $\approx 10^{14}$ W/cm^2 in silica [22], and voids issued from micro-explosions are created inside the irradiated volume. Alternatively, another regime is commonly defined in the literature, labeled "heat accumulation regime". The latter is achieved at high repetition rate of the fs-laser system. This regime corresponds to the conditions where the inter-pulse period approaches or becomes shorter than the heat diffusion time needed to fully evacuate the heat deposited after each pulse. This causes a net temperature increase from pulse to pulse, and a spatial broadening of the fs-laser modified area with a size that overcomes the beam size itself (provided the deposited energy is high enough) [24]. However when discussing the energy thresholds, it is not accurate to speak about heat accumulation threshold, but rather about a temperature threshold and its spatial extension. More details are provided later in this article.

The most common macroscopic photosensitive response desired is a refractive index modification with a strong index contrast (Δn, Type I), which can subsequently be employed to inscribe 3D free form objects and functions, such as Bragg filters, waveguides, and diffractive or exponential gradient planar lenses. In this paper we will therefore focus on this regime. In the literature, only few studies report on the photosensitivity of BGG glasses by fs-lasers. The first one, in 2017, investigated fs-response of a **BGG** with a molar composition of 12.5%BaO – 75%GeO_2 – 12.5%Ga_2O_3, and the authors obtained a maximum positive refractive index contrast (Δn) of 8×10^{-3} with respect to the pristine glass, after varying both scanning speed and pulse energy. In the same study, the authors investigated the effect of glass composition on its photosensitivity, in x%BaO – (100-2x)%GeO_2 – x%Ga_2O_3 glass molar

compositions, with x taking values of 20%, 17.5%, 12.5%, and 7.5%; each glass exhibited a similar response upon fs-laser irradiation. Very recently, the same team showed the possibility to inscribe waveguides in a 17.5%BaF_2 – 17.5%Ga_2O_3 – 65%GeO_2 glass and managed to obtain a Δn of $\approx 3\times10^{-3}$ [25]. Addition of a halogen component has the effect to mitigate water content during the glass synthesis [26]. However, the Δn is reduced by approximately 60% with respect to its all-oxide counter-part [25].

In this work, we investigate the photosensitivity of 6 BGG glasses, labeled GGK, BGGLaY1, BGGLaY2, BGGLaY3, BGGK, BGGN with capitalized letters corresponding to the principal cation species presented in the respective glass compositions. The latter are provided in Table 1. These modified BGG glass compositions would present good assets between relatively high nonlinear optical properties, important hardness, high transition temperature, and fiber drawing ability, in particular for yttrium- and lanthanum-containing glasses [27, 28].

Table 1. Label, molar composition, and physical characteristics of the BGG glass samples

Sample	Composition (%)	T_g ($\pm$5°C)	n_{532nm} ($\pm$0.01)
GGK	25Ga_2O_3 - 50GeO_2 - 25K_2O	661	1.63
BGGLaY1	21Ga_2O_3 - 43GeO_2 - 24BaO - 6La_2O_3 - 6Y_2O_3	728	1.805
BGGLaY2	15Ga_2O_3 - 60GeO_2 - 13BaO - 6La_2O_3 - 6Y_2O_3	736	1.796
BGGLaY3	28Ga_2O_3 - 37GeO_2 - 23BaO - 6La_2O_3 - 6Y_2O_3	735	1.780
BGGK	30Ga_2O_3 - 35GeO_2 - 24BaO - 11K_2O	642	1.701
BGGN	29Ga_2O_3 - 39GeO_2 - 23BaO - 9Na_2O	671	1.725

2. Experimental

A. Glass synthesis

These BGG samples were prepared through conventional melt-quenching technique from high purity reagents (Ga_2O_3: 99.998%, Strem Chemical, GeO_2: 99.999%, Strem Chemical, $BaCO_3$: 99.95%, Alfa Aesar, K_2CO_3: 99%, Sigma Aldrich, La_2O_3: 99.9%, Sigma Aldrich, Y_2O_3: 99.9%, Alfa Aesar and Na_2CO_3: 99.95%, Sigma Aldrich). The reagent grade $BaCO_3$ decomposed at high temperatures to form BaO. The powder precursors were mixed in a platinum crucible and melted at a temperature of 1300 °C for 30 min. The liquid was then quenched onto a metal plate to room temperature.

B. Pristine glass characterization

The glass transition temperatures (T_g) were measured by differential scanning calorimetry (DSC) and differential thermal analysis (DTA) Netzsch Pegasus 404 apparatus and with glass chunks inserted in a Pt pan, at a heating rate of 10 °C/min. The refractive indices (n_d) were characterized by the prism coupling method on an M-line Metricon 2010/M at 532 nm. Both T_g and n_d are reported in Table 1. Micro-Raman spectra were recorded in backscattering mode on a confocal micro-Raman spectrometer HR (Horiba / Jobin Yvon) equipped with a Synapse CCD detector using 532 nm excitation wavelength. The room temperature optical transmission measurements for each glass sample, in the UV-Visible-NIR and the IR ranges, were respectively obtained from Agilent Cary 5000 and Bruker Equinox 55 spectrophotometers. From the attenuation measurements, the absorption coefficients (α, in cm^{-1}) of the glass samples were calculated using sample thickness of 1 mm. Note that α was obtained after calculating internal transmittance $T_{int}(\lambda)$ [29] in order to remove the Fresnel losses. This further allow to calculate the excess loss Δα between before and after irradiation.

C. Fs-laser irradiation and characterization of modified regions

The glass samples, individually double-side polished to an optical grade, were placed on a translation stage for subsequent fs-laser irradiation. A commercial Yb-doped fiber amplifier fs-laser (Satsuma, Amplitude Systèmes Ltd. Pessac, France.) was used, with the following conditions: pulse duration = 300 fs; wavelength (λ) = 1030 nm; numerical aperture (NA) = 0.6; focusing depth = 300 µm. The beam size was defined by its lateral and longitudinal waist, respectively noted w_r and w_z. Moreover, the repetition rate and the pulse energy were varied. The inscription patterns inscribed in all samples were a series of rectangles with the dimensions of 100×10 μm^2. Each rectangle was in fact composed of a series of 10 lines being 100 µm long and with a spacing Δy of 1 µm. We used a constant pulse density $\boldsymbol{f/v}$ = 1000 pulses/µm, with $\boldsymbol{f}$ being the pulse repetition rate (Hz, or pulses/s) and $\boldsymbol{v}$ the scanning speed (µm/s). The repetition rate $\boldsymbol{f}$ was varied between 20 kHz to 400 kHz and, therefore, the laser scanning speed was varied from 20 µm/s to 400 µm/s accordingly. Moreover, the pulse energy $\boldsymbol{E_p}$ was also varied, from 0.025 to 5 µJ. Finally, the linear laser polarization was oriented parallel to the laser scanning direction.

Following the laser irradiation, each sample was placed on an Olympus BX51 polarized optical microscope. In addition to a typical optical microscope observation, each sample was investigated using quantitative phase microscopy (QPM, Iatia). This technique measures the phase retardation (Δφ, in rad) caused by the irradiated object with respect to the surrounding pristine glass. From this measurement, the refractive index modifications can be calculated through the following relationship: $\Delta n = \frac{\Delta\varphi\lambda}{2\pi d}$, where $\boldsymbol{\lambda}$ is the wavelength of the illuminating microscope light (550 nm), and $\boldsymbol{d}$ is the thickness of the modified region.

3. Results and discussions

Figure 1(a) displays the Raman spectra normalized to the total scattered intensity cross-section from 200 to 1400 cm^{-1}. The Raman spectra confirmed the glass nature of all samples. Moreover, and for completeness, the principal band at the vicinity of 500-550 cm^{-1} corresponds to vibrations of X-O-X (X = Ga or Ge) bonds from connected tetrahedral XO_4 units [30]. It is worth noticing that the signature of vibrations involving Ga or Ge cations cannot be distinguished by Raman spectroscopy due to their similar masses.

The two bands centered at 780 cm^{-1} and 870 cm^{-1} for GGK glass are attributed to stretching modes of Ge and Ga tetrahedral units, respectively. They are likely in an annular configuration or chain in which the charge on oxygen varies depending on the location of the potassium compensating charge cations. For all glasses beside GGK, a band located around 830 cm^{-1} is observed. For all these compositions, the charge compensation of gallium oxide tetrahedra is guaranteed by the sufficient amount of positive charges Na^{+}, K^{+}, Ba^{2+}, Y^{3+} or La^{3+} and the excess leads to the formation of non-bridging oxygens (NBOs) vibrating at 830 cm^{-1}. Here, the introduction of the excess cations promotes the formation of NBOs with the depolymerization of gallium oxide based glass network [31]. The positive charge ratio of modifiers versus Ga can be estimated as follows: (2Ba+3La+3Y+Na+K)/Ga, and without taking into account the real charge compensation ability of each cation. Following this, the ratio is in the following order: BGGLaY2 (3.24), BGGLaY1 (2.84), BGGLaY3 (2.11), BGGK (1.19), BGGN (1.12), and GGK (1.00). Moreover, the remaining Ba^{2+}, Y^{3+} and La^{3+} (i.e., which do not compensate the charge of $[GaO_4]^{-}$ polyhedra), participate

in the formation of NBOs on GeO_4 units [18]. The slight shift of the 830 cm^{-1} band position is thus attributed to the nature of the cation modifier involved.

Figure 1(b) presents the absorption coefficient measurements for each glass sample. Two broad absorption bands can be observed at 3 µm and 5 µm. They correspond to the two broad asymmetric absorption bands assigned to the hydroxyl (OH) stretching vibrations due to the absence of purification steps during the glass synthesis. Previously a deconvolution with four Gaussian bands has been proposed in the Ga_2O_3–GeO_2–BaO glass system, where the highest frequency ones are attributed to Ga–OH and Ge–OH vibrations (free hydroxyl), while the lowest ones may be attributed to either T – O – H – O (T= Ga or Ge) strong, or very strong, hydrogen bonds [32]. Other authors have proposed, for tellurite glasses, that the vibrations around 5 µm could be due to the overtone of OH bending modes [33]. One can notice that the glasses exhibiting the highest germanate content also present the highest intensity OH-associated vibrations. This effect may be related to the purity of the germanium oxide precursor but also its hydrophilic nature.

The IR multiphonon cut-off is made up of a peak at 6.25 µm and a strong absorption edge above 7 µm. There are two main points to discuss: the effect of modifiers as well as the Ga/Ge ratio on the position of the IR cut-off. The origin of the multiphonon absorption edge can be difficult to elucidate. Thus, various aspects must be taken into consideration, such as the rare-earth/Ba content and their atomic mass, the harmonic combinations of fundamental vibrational modes or the overtone of OH vibrations. The peak at 6.25 µm seems to decrease when the Ga/Ge ratio increases and where the band associated to Q^3 GeO_4 units decreases. The IR spectra show a signature of the band associated to Q^3 GeO_4 units located at 800 cm^{-1}, which could lead to an overtone in the 6 µm spectral region [30].

The fabrication of Mid-IR photonic devices will require first reducing the OH content and if possible, avoiding Q^3 units to benefit from an extended IR transmission.

Insert Fig. 1 here

Insert Fig. 2 here

Figure 2 displays the various types of modifications, in a pulse energy – repetition rate landscape, induced by fs-laser irradiation for BGGLaY1 glass sample and characterized by optical microscopy. The other glass samples follow similar trends and the BGGLaY1 is consequently provided as an exemplar of the typical features being observed. The pulse energy – repetition rate is framed between several contributions that dictate the glass photosensitivity. At very low energies (<0.20μJ), there are no permanent modifications detected in the glass. As the energy is progressively increased (moving vertically upward in Figure 2), we observe the onset of Type I modification. This corresponds to an isotropic and positive phase change (hence refractive index increase) with respect to the pristine glass. This Type I corresponds to the data points in blue in the Figure 2. This regime is opposed to the so-called "transition regime" and "spatial broadening regime" in a sense that there is no broadening of the laser track. This is particularly attractive to imprint compact and highly localized photo-induced transformations. The observable laser track broadening arises from two different origins depending if one moves vertically (increasing pulse energy, case 1) or horizontally (increasing repetition rate, case 2).

A. Case 1

At low repetition rate, when we increase the pulse energy, $\boldsymbol{E_p}$, the spatial distribution of the temperature profile is unchanged according to the heat equation (Fourier's law). However, the deposited heat also increases, and so does the maximum temperature ($\boldsymbol{T_{max}}$) in the focal volume (yet there is no more heat build-up from pulse-to-pulse). The maximum temperature in the pulse center is $T_{max} = \frac{AE_p}{\pi\rho C_p w_r{}^2 w_z}$ [34] where $A \times E_p$ is the energy absorbed per unit volume ($\boldsymbol{A}$ is the absorbed fraction), and $\boldsymbol{\rho}$ and $\boldsymbol{C_p}$ are the glass density and the heat capacity, respectively. The $\boldsymbol{T_{max}}$ elevation as $\boldsymbol{E_p}$ increases leads to an enlarged spatial volume within which the local temperature is higher than a transformation temperature, i.e., a temperature threshold (here corresponding to an observable positive and permanent refractive index change).

B. Case 2

When the repetition rate ***f*** increases, the spatial temperature profile changes from Gaussian to Lorentzian-Gaussian (Gaussian in the center, Lorentzian in the periphery). This has the consequence to decrease the width at half height of the temperature profile, and therefore this is not what widens the laser track. Instead, here the heat accumulation increases the amplitude, since now the expression of the maximum temperature can be describe as $T_{max} = \frac{3A.E_p f}{8D\pi\rho C_p w}$ and thus the imprinted width for a given temperature that can overcome the laser beam size (w_r and w_z) by several orders of magnitude.

Following this view, the minimum time ($\boldsymbol{\tau_{min}}$) needed to evacuate 90% of the heat deposited within the focal volume can be approximated by the following formula: $\tau_{min} \approx w_0^2/D$, where $\boldsymbol{w_0}$ is the beam waist radius, ***D*** the thermal diffusion coefficient, expressed as $D = \kappa/(\rho \cdot C_p)$, and with ***k*** being the thermal conductivity. In our conditions $w_r \approx 1$ µm. For a typical germanate glass (e.g., Schott IRG-2), one can estimate ***D*** as $3.7 \cdot 10^{-7}$ m²/s [35]. This leads to a $\tau_{min} \approx 2.7$ µs. To provide a comparison, for silica glass ($D \approx 9 \cdot 10^{-7}$ m²/s) we obtain $\tau_{min} \approx 1.1$ µs. These values translate to frequencies of ≈ 370 kHz and ≈ 890 kHz for germanate and silica glasses, respectively. These calculations provide a crude estimate about the frequency onset of heat accumulation caused by an increase in the repetition rate, and show that it is expected to be much lower than what is found for silica glass. This is in a quite good agreement with trends observed in the Figure 2, indicating that the spatial broadening regime is likely due to heat-accumulation that becomes preponderant in the 200-400 kHz.

Now that the types of fs-laser induced modifications are identified and described, we focus to the amplitude of the phase shift, hence refractive index contrast, generated during the laser irradiation. The evolution of the phase shift as a function of the pulse energy, for each glass sample, is displayed in the Figure 3. Here we chose to display the data measured at a repetition rate of 100 kHz since we can best observe the transition from the Type I to the spatial broadening regime (see Figure 2). We distinguish two groups of glasses: GGK, BGGK and BGGN and BGGLaY1, BGGLaY2, and BGGLaY3 in the Figure 3 (a) and (b), respectively. The first group the glasses contain varying amount of alkali (K and Na), while in the

second group the Ge-Ga-Ba proportions are varied. Overall, we observe a positive phase shift, starting from Type I onset, increasing with pulse energy and until it reaches a plateau. The maximum Δφ measured in our conditions exceeded 8 rad for GGK glass, and with a maximum value of 8.7 rad for BGGLaY3 in Figure 3(b). Some features are common to all glass samples. At low pulse energies (< 2 μJ), each group has a similar Δφ response. However, beyond 2 μJ, we observe discrepancies in the Δφ magnitude. In Figure 3(a), comparing BGGN and BGGK, it appears that the addition of K atoms in the glass promotes higher phase shifting compared to the Na-containing glass for pulse energies > 3 μJ. The variation could be related to the fictive temperature effect, i.e., the dependency between viscosity and cooling rate. In the Type I regime, the magnitude of the phase shift is not sufficient to observe composition dependence, the signal to noise ratio being too weak. In the heat accumulation region, corresponding to pulse energy above 2 μJ, the situation is clearer. The maximum phase shift in the spatial broadening regime (Δφ in the 6 - 8 rad region) was higher than that in Type I regime indicating the prime candidate of BGG glasses for the inscription of waveguides.

Insert Fig. 3 here

Figure 4 shows the maximum phase shift measured through QPM system as a function of Cations/$GaO_{3/2}$ (in cationic mol%) within the 6 studied glasses. Herein, we will limit our interpretation only to the spatial broadening regime. Figure 4 helps us to establish a link between the phase shift and the structural network in glasses. Hypothetically, the origin of the phase shift could be different between the rare earth and alkali-containing BGG glasses, therefore the data are discussed separately. Overall, the maximum phase shift decreased with the value of Cations/$GaO_{3/2}$ (in cationic mol%, Cations: 2Ba+3La+3Y+Na+K). For the rare-earth-containing glasses, the trend of Δφ is obvious; it increases in the following order: BGGLaY3 > BGGLaY1 > BGGLaY2. One should note that the nature and concentrations and ratio of La and Y were kept constant. Note that the aforementioned order is preserved in terms of $GaO_{3/2}/GeO_2$, but is reversed in terms of the number of NBOs before laser irradiation.

On the contrary, for the alkali-containing ones, we changed the nature of cation modifiers and their concentrations. GGK glass exhibited the maximum phase shift, and is the glass sample that possesses a ratio

of Cations/$GaO_{3/2}$ equals to 1, or in other words the K atoms only occupy charge-compensating sites. Comparing GGK to both BGGK and BGGN glasses, one can see that Δφ decreased upon the introduction of Q^3 germanate units. This result highlights the importance of the charge compensation aspect concerning its effect on the phase shift. Thus, charge compensation in the network may help in the mobility of modifiers, probably inducing a higher refractive index variation.

For all studied compositions, we conclude that a lower number of NBO units (i.e., more charge compensating cations), leads to an increased value in the phase shift.

Insert Fig. 4 here

Insert Fig. 5 here

Furthermore, the excess losses post fs-laser irradiation at 2500 nm for GGK, BGGLaY1, BGGLaY2 and BGGLaY3 glasses were measured using a FTIR spectrometer and are provided in Figure 5. Above 1.5 μJ, the excess losses increased along with pulse energy, which can be explained by the inhomogeneities that can be seen in the optical microscope images, resulting in high light scattering. However, the excess losses remain below 2 cm^{-1} for a fixed phase shift of π rad (a useful arrange for optical applications).

Finally, a review of the refractive index changes Δn measured in BGG, Fluoride, Chalcogenide, Germanate and SiO_2 glasses is shown in Figure 6 (data collected from Refs. [36-42]). Using imprinted the laser track lengths measured by optical microcopy we deduce the Δn from Δφ. The Δn of BGG glasses ranges up to 1.54×10^{-2} and were comparable to most chalcogenide glasses, and much higher than fluoride glasses. With the range of refractive index from 1.63 to 1.805 and the quite high Δn, BGG glasses exhibit a high potential and appear competitive compared to most chalcogenide glasses for Mid-IR applications.

Insert Fig. 6 here

4. Conclusions

A quick overview of the photosensitivity of high optical transparency (0.5 to 5.5 μm) BGG glasses exposed to IR-fs laser light was presented. The results in energy−repetition rate window evidenced that above a

certain temperature threshold, a drastic increase of refractive index change Δn was observed that correlates with a spatial broadening of the laser tracks. According to the comparison made in 6 BGG glasses particularly in the spatial broadening regime, the ratio of Cations/$GaO_{3/2}$ (cationic mol %) significantly impacts the maximum refractive index changes of the irradiated areas which become more important due to the charge compensation aspect and lower amount of NBOs on GeO_4 units, resulting in higher index changes. Our results clearly demonstrated the potential of BGG glasses as prime candidates for the development of embedded photonic devices in the Near-IR and Mid-IR including graded index optics, diffractive optics and 3D geometric phase optics.

Funding

This work is financially supported by Agence Nationale de la Recherche (ANR-18-CE08-0004-01); FLAG-IR Project; National Natural Science Foundation of China (11774220, 61735010); Science and Technology Innovation Plan of Shanghai Science and Technology Commission (20JC1415700).

Disclosures

The authors declare no conflicts of interest.

References

[1] B. Zhang, D. Tan, Z. Wang, X. Liu, B. Xu, M. Gu, L. Tong, J. Qiu, Self-organized phase-transition lithography for all-inorganic photonic textures, Light: Science & Applications, 10 (2021) 93.

[2] K. Miura, J. Qiu, H. Inouye, T. Mitsuyu, K. Hirao, Photowritten optical waveguides in various glasses with ultrashort pulse laser, Applied Physics Letters, 71 (1997) 3329.

[3] J. Bérubé, A. Camus, S. Messaddeq, Y. Petit, Y. Messaddeq, L. Canioni, R. Vallée, Femtosecond laser direct inscription of mid-IR transmitting waveguides in BGG glasses, Optical Materials Express, 7 (2017) 3124-3135.

[4] Y. Bellouard, A. Said, P. Bado, Integrating optics and micro-mechanics in a single substrate: a step toward monolithic integration in fused silica, Optical Express, 13 (2005) 6635–6644.

[5] K. Davis, K. Miura, N. Sugimoto, K. Hirao, Writing waveguides in glass with a femtosecond laser, Optical Letters, 21 (1996) 1729–1731.

[6] Y. Sikorski, A. Said, P. Bado, R. Maynard, C. Florea, K. A. Winick, Optical waveguide amplifier in Nd-doped glass written with near-IR femtosecond laser pulses, Electronics Letters, 36 (2000) 226–227.

[7] A. Streltsov, N. Borrelli, Fabrication and analysis of a directional coupler written in glass by nanojoule femtosecond laser pulses, Optics Letters, 26 (2001) 42–43.

[8] T. Meany, M. Gräfe, R. Heilmann, A. Perez-Leija, S. Gross, M. Steel, M. Withford, A. Szameit, Laser written circuits for quantum photonics, Laser & Photonics Reviews, 9 (2015) 363–384.

[9] C. Athanasiou, Y. Bellouard, A monolithic micro-tensile tester for investigating silicon dioxide polymorph micromechanics, fabricated and operated using a femtosecond laser, Micromachines, 6 (2015) 1365–1386.

[10] T. Zhou, L. Fang, T. Yan, J. Wu, Y. Li, J. Fan, H. Wu, X. Lin, Q. Dai, In situ optical backpropagation training of diffractive optical neural networks, Photonics Research, 8 (2020) 940-953.

[11] S. Eaton, M. Ng, R. Osellame, P. Herman, High refractive index contrast in fused silica waveguides by tightly focused, high-repetition rate femtosecond laser, Journal of Non-Crystalline Solids, 357 (2011) 2387–2391.

[12] J. Bérubé, S. Messaddeq, I. Skripachev, R. Vallée, Y. Messaddeq, Tailoring the refractive index of Ge-S based glass for 3D embedded waveguides operating in the mid-IR region, Optics Express, 22 (2014) 26103–26116.

[13] W. Ma, P. Zhang, W. Zhou, Q. Qi, Z. Wu, L. Wang, W. Zhang, B. Song, S. Dai, Femtosecond-laser direct-writing volume phase gratings inside Ge-As-S chalcogenide glass, Ceramics International, 46 (2020) 17599-17605.

[14] L. Liu, F. Chen, J. Cui, X. Xiao, Y. Xu, C. Hou, X. Cui, H. Guo, The mutual influence between rare earth element doping and femtosecond laser-induced effects in Ga-As-Sb-S chalcogenide glass, Ceramics International, 47 (2021) 6388-6396.

[15] S. Gross, N. Jovanovic, A. Sharp, M. Ireland, J. Lawrence, M. Withford, Low loss mid-infrared ZBLAN waveguides for future astronomical applications, Optics Express, 23 (2015) 7946–7956.

[16] J. Bai, X. Long, X. Liu, G. Huo, W. Zhao, R. Stoian, R. Hui, G. Cheng, Embedded optical waveguides fabricated in SF10 glass by low-repetition-rate ultrafast laser, Applied Optics, 52 (2013) 7288–7294.

[17] T. Skopak, F. Calzavara, Y. Ledemi, F. Célarié, M. Allix, E. Véron, M. Dussauze, T. Cardinal, E. Fargin, Y. Messaddeq, Properties, structure and crystallization study of germano-gallate glasses in the Ga_2O_3-GeO_2-BaO-K_2O system, Journal of Non-Crystalline Solids, 514 (2019) 98-107.

[18] S. Bayya, G. Chin, J. Sanghera, I. Aggarwal, Germanate glass as a window for high energy laser systems, Optics Express, 14 (2006) 11687–11693.

[19] X. Wen, G. Tang, J. Wang, X. Chen, Q. Qian, Z. Yang, Tm^{3+} doped barium gallo-germanate glass single-mode fibers for 2.0 μm laser, Optics Express, 23 (2015) 7722-7731.

[20] X. Wen, G. Tang, Q. Yang, X. Chen, Q. Qian, Q. Zhang, Z. Yang, Highly Tm^{3+} doped germanate glass and its single mode fiber for 2.0 μm laser, Scientific Reports, 6 (2016) 20344.

[21] Y. Shimotsuma, P. G. Kazansky, J. Qiu, K. Hirao, Self-organized nanogratings in glass irradiated by ultrashort light pulses, Physical Review Letters, 91 (2003) 247405.

[22] E. Glezer, E. Mazur, Ultrafast-laser driven micro-explosions in transparent materials, Applied Physics Letters, 71 (1997) 882.

[23] M. Lancry, B. Poumellec, A. Chahid-Erraji, M. Beresna, P. Kazansky, Dependence of the femtosecond laser refractive index change thresholds on the chemical composition of doped-silica glasses, Optical Materials Express, 1 (2011) 711-723.

[24] S. Eaton, H. Zhang, P. Herman, F. Yoshino, L. Shah, J. Bovatsek, A. Arai, Heat accumulation effects in femtosecond laser-written waveguides with variable repetition rate, Optics Express, 13 (2005) 4708-4716.

[25] A. Camus, Y. Petit, J. Bérubé, M. Bellec, L. Canioni, R. Vallée, Direct-laser-written integrated mid-IR directional couplers in a BGG glass, Optics Express, 29 (2021) 8531-8541.

[26] S. Bayya, J. Sanghera, I. Aggarwal, Optical transmission of BGG glass material, U. S. patent 7,285,509B2 (23 October 2007).

[27] T. Guérineau, C. Strutynski, T. Skopak, S. Morency, A. Hanafi, F. Calzavara, Y. Ledemi, S. Danto, T. Cardinal, Y. Messaddeq, Extended germano-gallate fiber drawing domain: from germanates to gallates optical fibers, Optical Materials Express, 9 (2019) 2437-2445.

[28] C. Strutynski, F. Calzavara, T. Guerineau, L. Loi, R. Laberdesque, J. Rampnoux, S. Morency, Y. Ledemi, Y. Petit, M. Dussauze, F. Désévédavy, F. Smektala, S. Danto, L. Canioni, Y. Messaddeq, E. Fargin, T. Cardinal, Heavy-oxide glasses with superior mechanical assets for nonlinear fiber applications in the mid-infrared, Optical Materials Express, 11 (2021) 1420-1430.

[29] H. Hoffmann, Encyclopedia of Materials: Science and Technology, pp. 6426-6441.

[30] T. Skopak, S. Kroeker, K. Levin, M. Dussauze, R. Méreau, Y. Ledemi, T. Cardinal, E. Fargin, Y. Messaddeq, Structure and properties of gallium-rich sodium germano-gallate glasses, Journal of Physical Chemistry C, 123 (2019) 1370-1378.

[31] K. Yoshimoto, A. Masuno, M. Ueda, H. Inoue, H. Yamamoto, T. Kawashima, Low phonon energies and wideband optical windows of La_2O_3-Ga_2O_3 glasses prepared using an aerodynamic levitation technique, Scientific Reports, 7(2017) 45600.

[32] J. Jewell, I. Aggarwal, Structural influences on the hydroxyl spectra of barium gallogermanate glasses, Journal of Non-Crystalline Solids, 181 (1995) 189-199.

[33] G. Guery, T. Cardinal, A. Fargues, V. Rodriguez, M. Dussauze, D. Cavagnat, P. Thomas, J. Cornette, P. Wachtel, J. Musgraves, K. Richardson, Influence of Hydroxyl Group on IR Transparency of Tellurite-Based Glasses, International Journal of Applied Glass Science, 5 (2014) 178-184.

[34] E. Muzi, M. Cavillon, M. Lancry, F. Brisset, R. Que, D. Pugliese, D. Janner, B. Poumellec, Towards a rationalization of ultrafast laser-induced crystallization in lithium niobium borosilicate glasses: the key role of the scanning speed, Crystals, 11 (2021) 290.

[35] M. J. Weber, Handbook of optical materials (Berkeley, 2002).

[36] A. Arriola, S. Gross, M. Ams, T. Gretzinger, D. Coq, R. Wang, H. Ebendorff-Heidepriem, J. Sanghera, S. Bayya, L. Shaw, M. Ireland, P. Tuthill, M. Withford, Mid-infrared astrophotonics: study of ultrafast laser induced index change in compatible materials, Optical Materials Express, 7 (2017) 698-711.

[37] S. Gross, D. Lancaster, H. Ebendorff-Heidepriem, T. Monro, A. Fuerbach, M. Withford, Femtosecond laser induced structural changes in fluorozirconate glass, Optical Materials Express, 3 (2013) 574-583.

[38] S. Messaddeq, J. Bérubé, M. Bernier, I. Skripachev, R. Vallée, Y. Messaddeq, Study of the photosensitivity of GeS binary glasses to 800 nm femtosecond pulses, Optics Express, 20 (2012) 2824-2831.

[39] M. Hughes, W. Yang, D. Hewak, Fabrication and characterization of femtosecond laser written waveguides in chalcogenide glass, Applied Physics Letters, 90 (2007) 131113.

[40] S. Eaton, M. Ng, R. Osellame, P. Herman, High refractive index contrast in fused silica waveguides by tightly focused, high-repetition rate femtosecond laser, Journal of Non-Crystalline Solids, 357 (2011) 2387-2391.

[41] S. Sebastiani, G. Nunzi Conti, S. Pelli, G. C. Righini, Characterization of a highly photorefractive RF-sputtered SiO_2-GeO_2 waveguide, Optics Express, 13 (2005) 1696-1701.

[42] J. Hu, N. Feng, N. Carlie, L. Petit, J. Wang, Low-loss high-index-contrast planar waveguides with graded-index cladding layers, Optics Express, 15 (2007) 14566-14572.

Figure captions:

Figure 1 (a) Normalized Raman Intensity of GGK, BGGLaY1, BGGLaY2, BGGLaY3, BGGK and BGGN glasses as a function of Raman shift. (b) Absorption coefficients of GGK, BGGLaY1, BGGLaY2, BGGLaY3, BGGK and BGGN glasses as a function of wavelength.

Figure 2 Pulse energy – repetition rate landscape and identification of Type I regime, transition regime and spatial broadening regime in BGGLaY1 glass.

Figure 3 (a) Phase shift (in rad) for GGK, BGGK and BGGN glasses as a function of pulse energy. (b) Phase shift for BGGLaY1, BGGLaY2 and BGGLaY3 glasses. Left inset: optical image of BGGLaY1 in low energy. Right inset: optical image of BGGLaY1 (3 μJ and 2.5 μJ from left to right). Lines are guide-to-the-eye.

Figure 4 Maximum phase shift ($\Delta\varphi$, in Rad) as a function of Cations/$GaO_{3/2}$ (in cationic mol%).

Figure 5 Excess loss at 2500 nm as a function of energy for GGK, BGGLaY1, BGGLaY2 and BGGLaY3 glasses after fs laser irradiation.

Figure 6 Ranges of refractive index variations induced by fs-laser vs. refractive index (typ. measured at 532 nm) for the BGG, chalcogenide, fluoride, SiO_2 and germanate glasses.

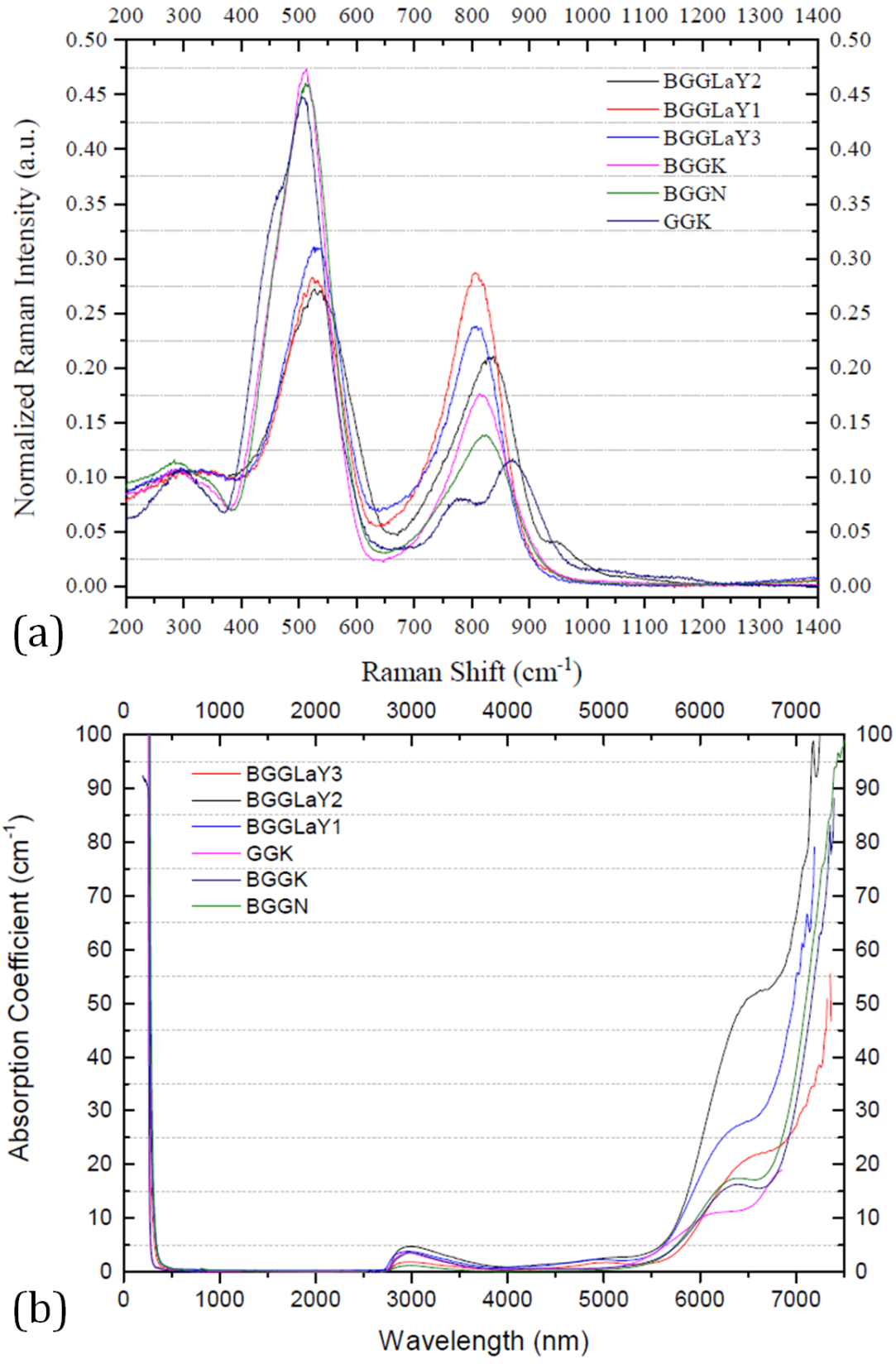
Normalized Raman Intensity (a.u.)
Raman Shift (cm-1)
BGGLaY2
BGGLaY1
BGGLaY3
BGGK
BGGN
GGK
(a)
Absorption Coefficient (cm-1)
Wavelength (nm)
BGGLaY3
BGGLaY2
BGGLaY1
GGK
BGGK
BGGN
(b)

Figure 1

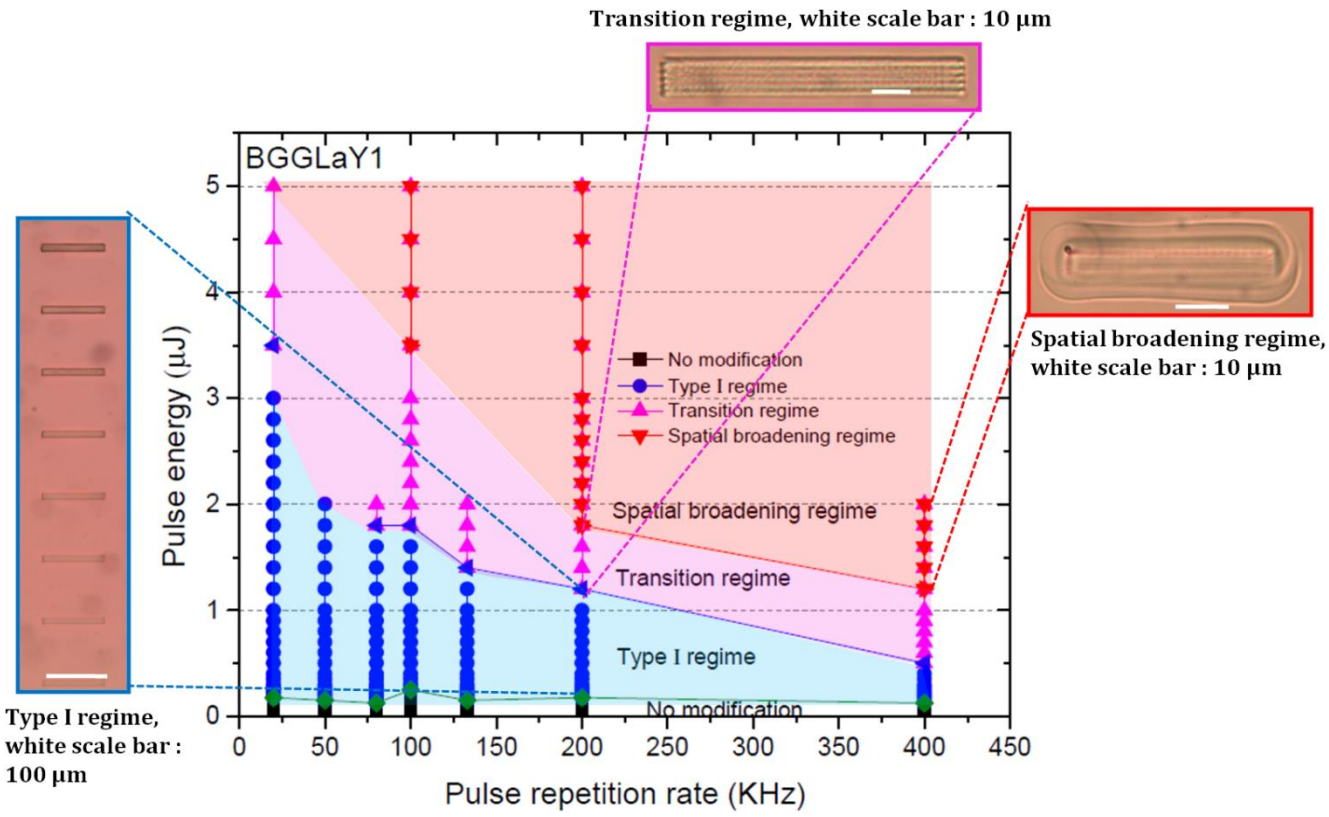
Transition regime, white scale bar : 10 µm
BGGLaY1
Pulse energy (µJ)
Pulse repetition rate (KHz)
No modification
Type I regime
Transition regime
Spatial broadening regime
Spatial broadening regime
Transition regime
Type I regime
No modification
Spatial broadening regime, white scale bar : 10 µm
Type I regime, white scale bar : 100 µm

Figure 2

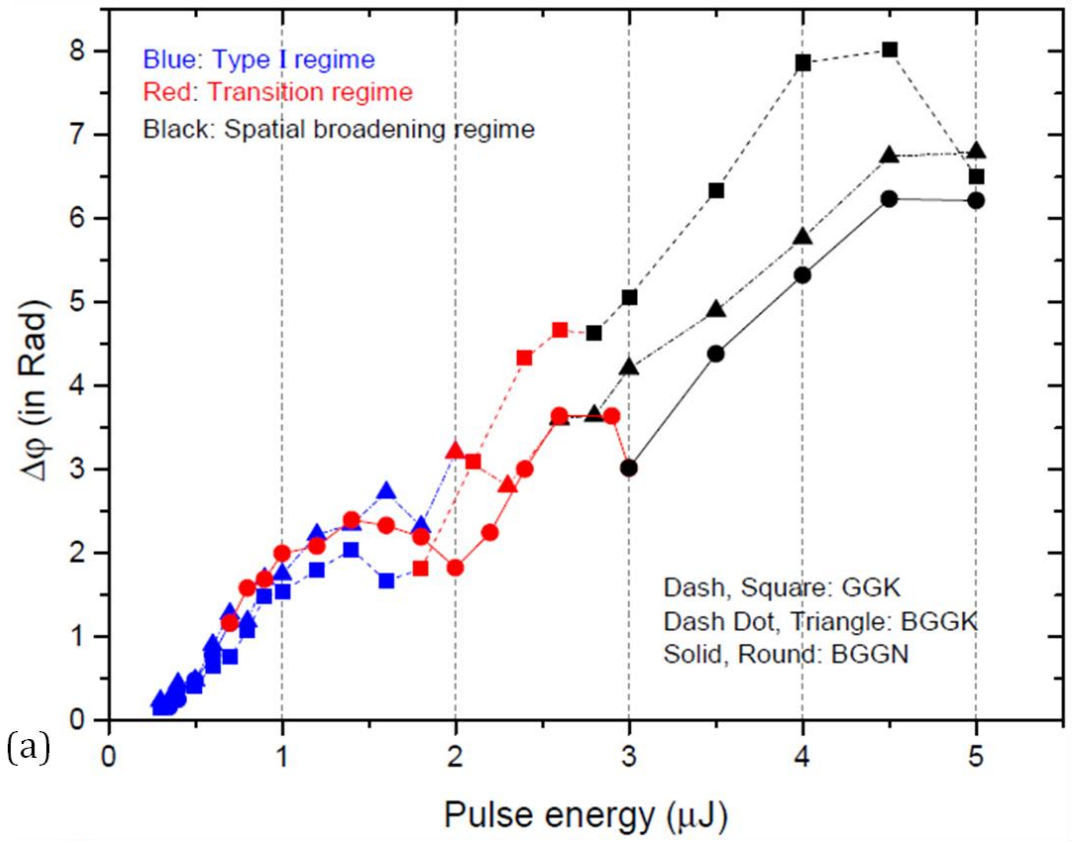
Blue: Type I regime
Red: Transition regime
Black: Spatial broadening regime
Dash, Square: GGK
Dash Dot, Triangle: BGGK
Solid, Round: BGGN
Δφ (in Rad)
Pulse energy (μJ)
(a)

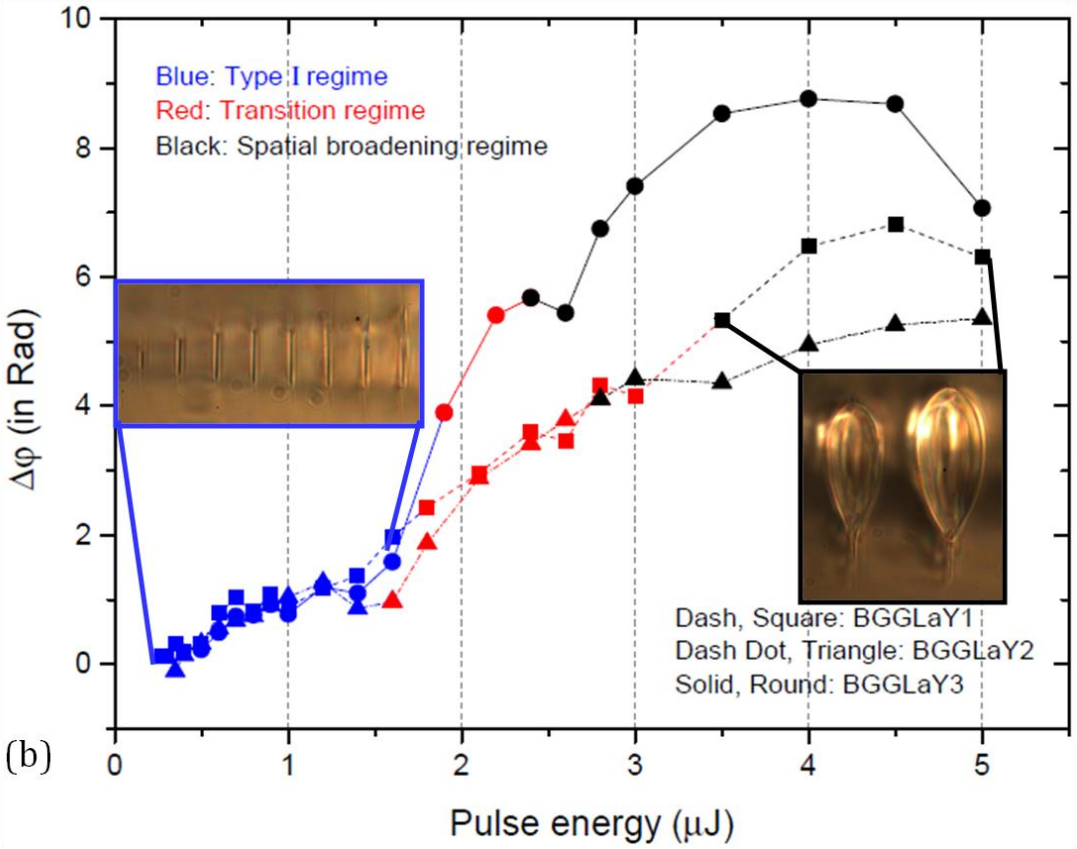
Blue: Type I regime
Red: Transition regime
Black: Spatial broadening regime
Dash, Square: BGGLaY1
Dash Dot, Triangle: BGGLaY2
Solid, Round: BGGLaY3
Δφ (in Rad)
Pulse energy (μJ)
(b)

Figure 3

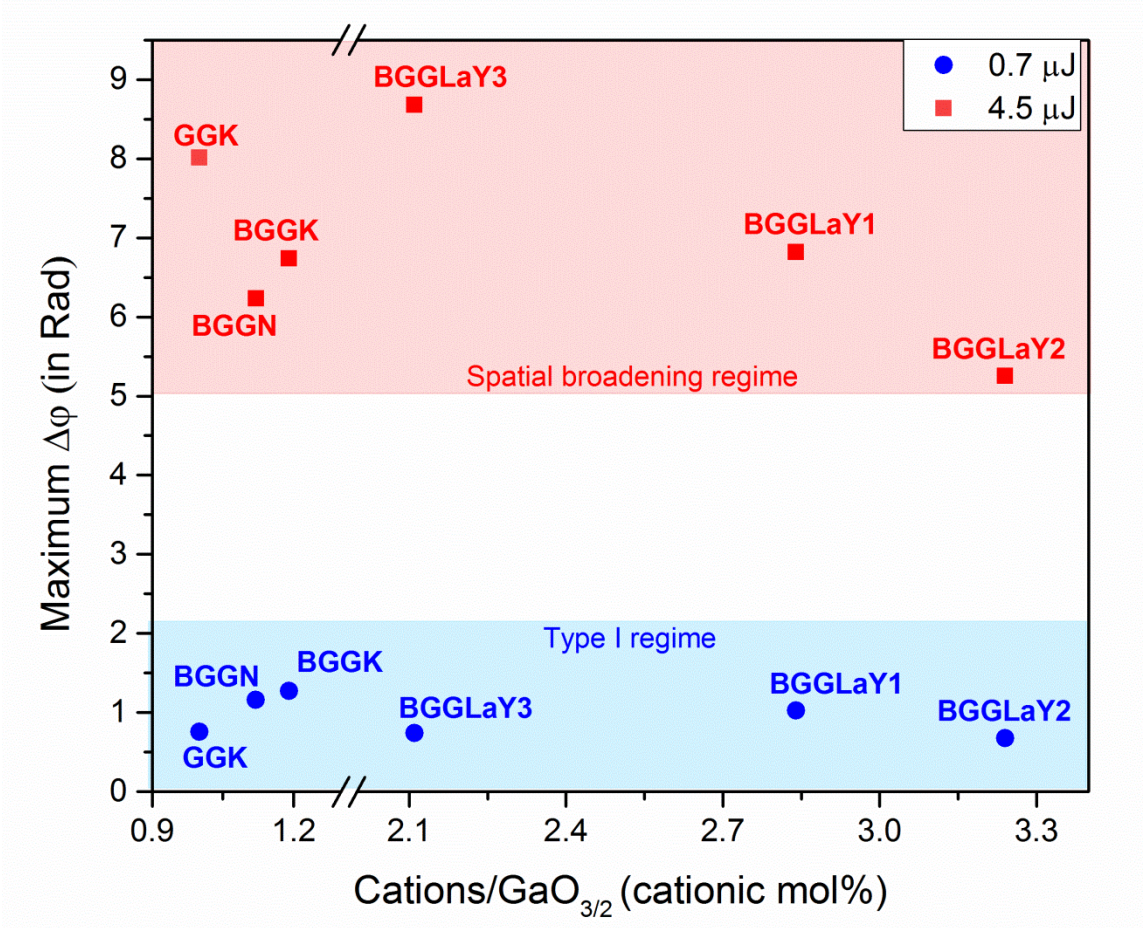
0.7 μJ
4.5 μJ
BGGLaY3
GGK
BGGK
BGGLaY1
BGGN
BGGLaY2
Spatial broadening regime
Type I regime
BGGN
BGGK
BGGLaY1
BGGLaY3
BGGLaY2
GGK
Maximum Δφ (in Rad)
Cations/GaO3/2 (cationic mol%)
0
1
2
3
4
5
6
7
8
9
0.9
1.2
2.1
2.4
2.7
3.0
3.3

Figure 4

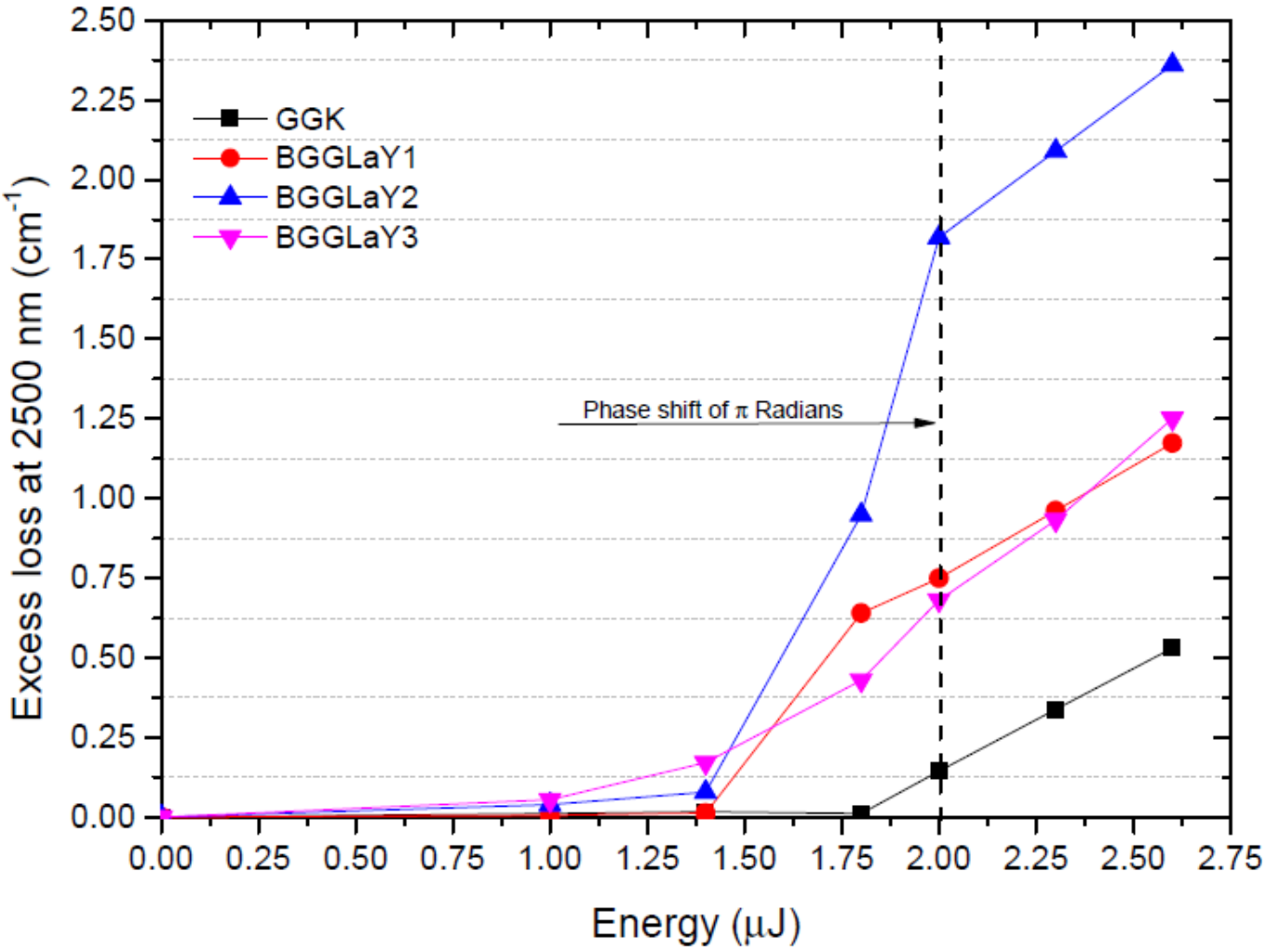
GGK
BGGLaY1
BGGLaY2
BGGLaY3
Phase shift of π Radians
Excess loss at 2500 nm (cm-1)
Energy (μJ)
0.00
0.25
0.50
0.75
1.00
1.25
1.50
1.75
2.00
2.25
2.50
2.75

Figure 5

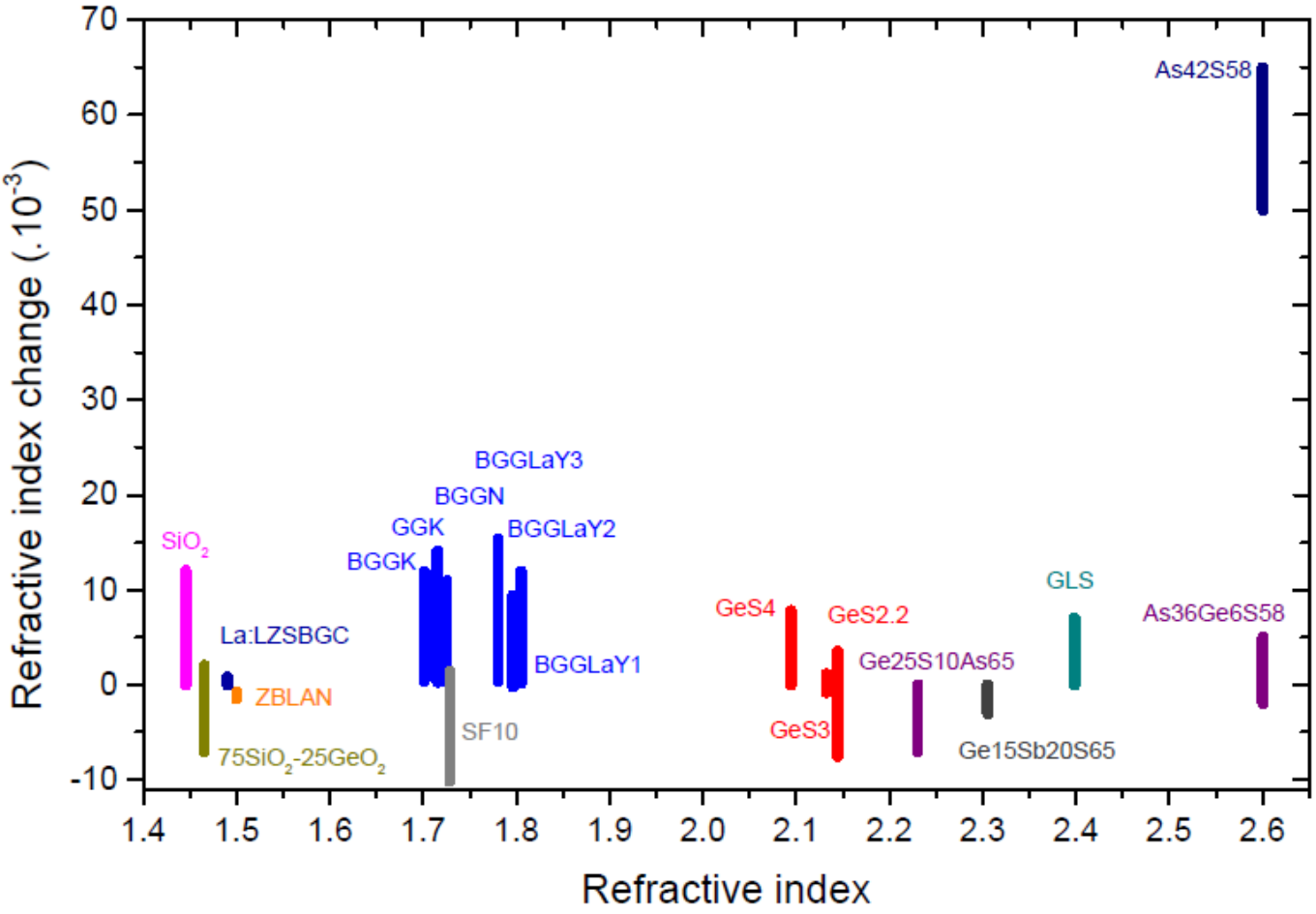
Refractive index change (.10-3)
Refractive index
70
60
50
40
30
20
10
0
-10
1.4
1.5
1.6
1.7
1.8
1.9
2.0
2.1
2.2
2.3
2.4
2.5
2.6
As42S58
BGGLaY3
BGGN
GGK
BGGLaY2
BGGK
SiO2
La:LZSBGC
ZBLAN
75SiO2-25GeO2
SF10
BGGLaY1
GeS4
GeS2.2
Ge25S10As65
GLS
As36Ge6S58
GeS3
Ge15Sb20S65

Figure 6